

Implications of the delayed 2013 outburst of the ESO 243-49 HLX-1

O. Godet^{1,2}

¹ *Institut de Recherche en Astrophysique and Planétologie (IRAP), Université de Toulouse, UPS, 9 Avenue du colonel Roche, 31028 Toulouse Cedex 4, France*

² *CNRS, UMR5277, 31028 Toulouse, France*

J. C. Lombardi³

³ *Department of Physics, Allegheny College, Meadville, PA 16335, USA*

F. Antonini⁴

⁴ *Canadian Institute for Theoretical Astrophysics, University of Toronto, 60 St. George Street, Toronto, Ontario M5S 3H8, Canada*

D. Barret, N. A. Webb^{1,2}

and

J. Vingless³, M. Thomas³

ABSTRACT

After showing four quasi-periodic outbursts spaced by ~ 1 year from 2009 to 2012, the hyper luminous X-ray source ESO 243-49 HLX-1, currently the best intermediate mass black hole (IMBH) candidate, showed an outburst in 2013 delayed by more than a month. In Lasota et al. (2011), we proposed that the X-ray lightcurve is the result of enhanced mass transfer episodes at periapsis from a donor star orbiting the IMBH in a highly eccentric orbit. In this scenario, the delay can be explained only if the orbital parameters can change suddenly from orbit to orbit. To investigate this, we ran Newtonian smooth particle hydrodynamical (SPH) simulations starting with an incoming donor approaching an IMBH on a parabolic orbit. We survey a large parameter space by varying the star-to-BH mass ratio ($10^{-5} - 10^{-3}$) and the periapsis separation r_p from 2.2 to 2.7 r_t with r_t , the tidal radius. To model the donor, we choose several polytropes ($\Gamma = 5/2$, $n = 3/2$, $\Gamma = 3/2$, $n = 2$, $\Gamma = 5/3$, $n = 2$ and $\Gamma = 5/3$, $n = 3$).

Once the system is formed, the orbital period decreases until reaching a minimum that may be shallow. Then, the period tends to increase over several periapsis passages due to tidal effects and increasing mass transfer, leading ultimately to the ejection of the donor. We show that the development of stochastic fluctuations inside the donor by adding or removing orbital energy from the system could lead to sudden changes in the orbital period from orbit to orbit with the appropriate order of magnitude of what has been observed for HLX-1. We also show that given the constraints on the BH mass ($M_{\text{BH}} > 10^4 M_{\odot}$) and assuming that the HLX-1 system is currently near a minimum in period of ~ 1 yr, the donor has to be a white dwarf or a stripped giant core. We predict that if HLX-1 is indeed emerging from a minimum in orbital period, then the period would generally increase with each passage, although substantial stochastic fluctuations can be superposed on this trend.

Subject headings: X-rays: individual(HLX-1) — X-rays: binaries — accretion, accretion disks — black hole physics — methods: numerical

1. Introduction

Stellar mass black holes (BHs) are known to be the remnants of stellar activity with masses typically ranging from $\sim 3 - 20 M_{\odot}$. At the other end, supermassive BHs are thought to be present in the core of most massive galaxies with masses typically ranging from $\sim 10^6 - 10^{10} M_{\odot}$. However, the way supermassive BHs formed is still poorly understood. Most theories agree that supermassive BHs we observe today have been formed from lighter BH seeds present in the early Universe. What differs between models is the growth mechanisms and the mass range of the BH seeds (e.g. Alexander & Hickox 2012). Super-Eddington accretion of matter onto massive stellar mass BHs of ~ 100 solar masses has been invoked to explain the growth of supermassive BHs (e.g. Kawaguchi et al. 2004). Other scenarios propose the mergers of BHs with masses $\sim 10^2$ to $\sim 10^5$ solar masses, the so-called intermediate mass BHs (IMBHs – Madau & Rees 2001). In some models, both mechanisms are expected to take place. In the IMBHs scenarios, a fundamental question is then to understand how to form and how such BHs evolve (Miller & Colbert 2004). Despite long and thorough searches over the past last decades in different astrophysical objects such as globular clusters (Pooley & Rappaport 2006; Strader et al. 2012) and the low-mass tail of AGN (e.g. Greene & Ho 2004), the observational evidence for their existence is weak.

The serendipitous discovery of 2XMM J011028.1–460421 (hereafter Hyper Luminous X-ray source - HLX-1) with XMM-Newton on 23 November 2004 in the outskirts of the edge-on spiral galaxy ESO 243–49 at a redshift of 0.0224 marked a milestone with the most secure identification of an IMBH (Farrell et al. 2009 – hereafter F09). Wiersema et al. (2010) confirmed the association of HLX-1 to ESO 243–49 (see also Soria et al. 2013). With a 0.2–10 keV unabsorbed luminosity reaching $1.3 \times 10^{42} \text{ erg s}^{-1}$ at peak, HLX-1 is the brightest Ultra Luminous X-ray source (ULX – Roberts 2007; Feng & Soria 2011) detected so far. Spectral modeling of X-ray data with sophisticated accretion disk models (Davis et al. 2011; Godet et al. 2012; Straub et al. 2014) and Eddington scaling of X-ray data (Servillat et al. 2011) gave us a range of mass estimates around $\sim 10^4 M_{\odot}$ and recent radio data provide an upper limit on the BH mass

of $9 \times 10^4 M_{\odot}$ assuming Eddington scaling (Webb et al. 2012). Multi-wavelength observations of HLX-1 over the past five years enabled us to show that HLX-1 displays several properties similar to those observed in stellar mass BH X-ray binaries (e.g. Remillard & McClintock 2006): i) regular outbursts with state transitions, but with X-ray luminosities orders of magnitude larger (Godet et al. 2009b; Servillat et al. 2011); ii) the first ever detection of radio transient emission in a ULX interpreted as discrete jet ejection events following the hard-to-soft transitions (Webb et al. 2012). In 2012, we ran a series of contemporaneous optical (VLT) and X-ray (*Swift*-XRT) observations over the rise of the outburst in order to put some constraints on the outburst mechanism. Our data showed the optical may rise just before the X-rays, the delay being shorter than a day (Webb et al. 2014).

The *Swift*-XRT (Gehrels et al. 2004; Burrows et al. 2005) light-curve from 2009 to 2013 shows Fast Rise and Exponential Decay (FRED) outbursts separated by an apparent recurrence time of nearly a year (see Figure 1). In Lasota et al. (2011 – hereafter L11), we investigated the possibility to explain these outbursts as well as the spectral evolution during outburst in the framework of the Dwarf Instability Model (DIM – e.g. Lasota 2001). We demonstrated that outbursts of HLX-1 *cannot* be due to the thermal-viscous instability given the source distance of 95 Mpc. Instead, we proposed that the X-ray light-curve is the result of enhanced mass transfer episodes from an evolved (Asymptotic Giant Branch) star orbiting the IMBH in a highly eccentric orbit when the star passing at periapsis is tidally stripped. Given the small delay between the optical and X-rays, we also stressed that the mass delivery radius is rather small implying in the framework of the L11 scenario that the orbit must be highly eccentric.

Recently, Miller et al. (2014 – hereafter M14) proposed a mass-transfer scenario based on wind-fed accretion onto an IMBH when the donor star passes at periapsis. This scenario shows several similarities with the model we proposed in L11. To be able to account for a peak accretion rate around $\dot{M}_{\text{peak}} \sim 10^{-4} M_{\odot} \text{ yr}^{-1}$, M14 estimated that the mass loss needed should be at least one order of magnitude larger than \dot{M}_{peak} . Such a high mass loss is far beyond the expected maxi-

mum mass loss for AGB stars. To circumvent this issue, M14 propose that the AGB star was first disrupted by the IMBH thus losing its envelope and leaving its core orbiting the IMBH. The bared core would then emit a strong wind driven by high radiation pressure. This scenario also presents some caveats that will have to be investigated in detail: i) even with the loss of its envelope, it is yet to be demonstrated that the star mass loss could reach $\dot{M}_{\text{peak}} \sim 10^{-3} M_{\odot} \text{ yr}^{-1}$; ii) How does this scenario account for the almost simultaneous outburst rise seen in X-rays and optical (Webb et al. 2014)?; iii) AGB stars are known to produce a lot of dust. So, such a high mass loss should result in a strong extinction in optical. Our optical data collected so far does not seem to support this idea (Farrell et al. 2012).

To be complete on alternative models for HLX-1, we note the recent work done by King & Lasota (2014) who made an analogy of HLX-1 behavior with the Galactic source SS433. Again, from this work it appears that a precise model fine-tuning needs to be done in order to account for some of the HLX-1 observational properties. We note that the model is unable to explain fully some of the most remarkable properties of HLX-1 (e.g. the spectral variation). This piece of work again emphasizes how unique is the HLX-1 system. However, a detailed analysis of this scenario will have to be done to show if it is viable or not.

In this paper, we report on data collected in 2013 showing a significant change in the HLX-1 behavior. Indeed, the X-ray outburst is delayed by more than a month compared to previous years (see Fig. 1). This corresponds to a recurrence time of more than 400 days since the last outburst peaking on 23rd August 2012.

The aim of the present paper is to improve our understanding of the HLX-1 nature using an alternative approach through Smoothed Particle Hydrodynamical (SPH) simulations. The present paper will focus on the eccentric binary scenario we proposed in L11. In a forthcoming paper, we will investigate in detail the M14 scenario. The paper is organized as follows: in Section 2, we describe the data reduction of the *Swift*-XRT data. In Section 3, we discuss the main features of the X-ray light-curve, especially the apparent annual decrease in the outburst duration and the average peak count rate from 2009 to 2012. In Section

4, we present the data collected in 2013 and we compare the results with those obtained in previous years. In Section 5, we discuss the constraints that the data collected so far put on the eccentric binary scenario. In Section 6, we present the SPH simulations we run in order to investigate the possible reasons of the outburst delay, the lifetime of such a system and the nature of the donor. We also discuss the role of stochastic fluctuations developing inside the donor star on the orbital period and the mass loss stripping as well as the role of artificial viscosity on our results. Section 7 is devoted to the concluding remarks.

2. Data analysis

The *Swift*-XRT Photon Counting data (ObsID 31287 & 32577), unless otherwise mentioned, were processed using the HEASOFT v6.14, the tool XRPIPELINE v0.12.8¹ and the calibration files (CALDB version 4.1). We used the grade 0-12 events, giving slightly higher effective area at higher energies than the grade 0 events, and a 20 pixel (47.2 arcseconds) radius circle to extract the source and background spectra using XSELECT v2.4c. The background extraction region was chosen to be close to the source extraction region and in a region where we are sure that there are no sources present in the XMM-Newton field of view. The ancillary response files were created using XRTEKARF v0.6.0 and exposure maps generated by XRTEXPOMAP v0.2.7. We fitted the spectra within XSPEC v12.8.1 (Arnaud et al. 1994) using the response file SWXPC0TO12S6_20010101V013.RMF. All the errors quoted below are given at a 90% confidence level for one parameter of interest (*i.e.* $\Delta\chi^2 = 2.706$). The source redshift being 0.0224 (Wiersema et al. 2010), we adopted a source distance of $d_L = 95$ Mpc using the cosmological parameters from the WMAP5 results ($H_0 = 71$ km s⁻¹ Mpc⁻¹, $\Omega_M = 0.27$ & $\Omega_{\Lambda} = 0.73$). The X-ray lightcurve was generated using the online lightcurve generator made available on the *Swift* UK website (Evans et al. 2009) and using a dynamical count binning of 20 counts per bin.

When the count statistics was enough, the spectra were grouped at a minimum of 20 counts per bin to provide sufficient statistics to use the χ^2 minimization technique. For data in the low flux

¹See <http://heasarc.gsfc.nasa.gov/docs/swift/analysis/>

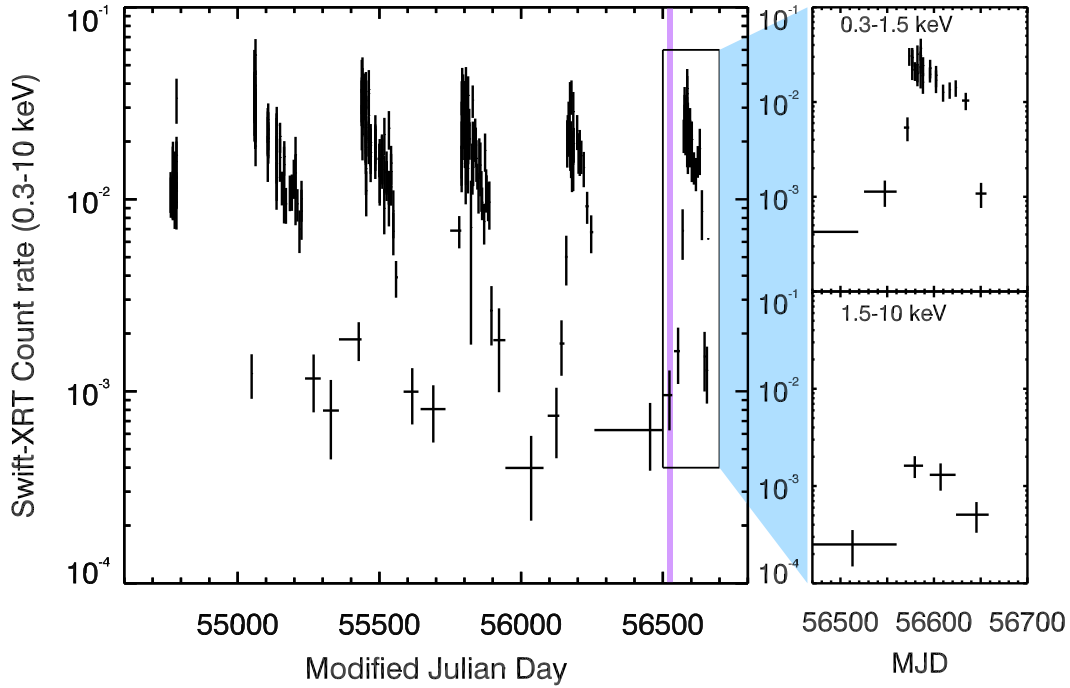


Fig. 1.— *Swift*-XRT Photon Counting lightcurve of HLX-1 in the 0.3-10 keV band from 24th October 2008 to 31st December 2013. The two panels on the right show a close-up of the X-ray lightcurve for the outburst in 2013: (top) in the 0.3-1.5 keV range; (bottom) in the 1.5-10 keV range. Since then, the source is in the low/hard state. The lightcurve was produced using the online lightcurve generator made available on the *Swift* UK website. We used a dynamical binning of 20 counts per bin. The vertical colored band corresponds to the time interval when the source was expected to enter in outburst in 2013 if it kept the timing observed from 2009 to 2012 (between 10th and 30th of August).

state, we used the C-statistic (Cash 1979) available within XSPEC for the spectral fit.

3. The X-ray lightcurve

We set up a monitoring of HLX-1 (PI: O. Godet) with the *Swift*-XRT through the *Swift* ToO program over 5 years in order to investigate in detail the temporal and spectral variability of the source as well as to trigger our multi-wavelength programs designed to investigate the nature of the HLX-1 host and how the BH is fed. Figure 1 shows the X-ray lightcurve from 24th October 2008 to 18th December 2013 for a total of 618.7ks so far. Below we summarize the main features seen in the X-ray lightcurve up to the outburst in 2012:

- i) Before 2012, the lightcurve displays 4 well sampled FRED-like outbursts with some re-flare events spaced by an apparent recurrence time of nearly a year (L11). The recurrence period appears to be variable (from ~ 350 to ~ 370 days). Since the serendipitous detection of HLX-1 with XMM-Newton in November 2004, at least 9 outbursts occurred assuming a recurrence time of nearly a year. Survey observations with *ROSAT* in the early nineties gave non-detections (Webb et al. 2010) indicating that either the source was in a low-flux state or in quiescence.
- ii) There is a 2-3 weeks plateau phase when the source reaches its outburst peak luminosity (L11; Godet et al. 2012).
- iii) When the source is not in outburst, it stays in the low/hard state (Godet et al. 2009; Servillat 2011).
- iv) The source switches rapidly (1-2 weeks) to the low/hard state when the 0.3-10 keV count rate is less than $\sim 7 \times 10^{-3}$ cts s^{-1} .
- v) The outburst duration decreases annually passing from ~ 170 days in 2009 to ~ 93 days in 2012, while the average peak count rate seems to have annually decreased even if it is more noticeable in 2012. Indeed, the average peak count rate was equal to 0.030 ± 0.002 cts s^{-1} in 2009, whereas it was equal to 0.020 ± 0.002 cts s^{-1} in 2012 (90% confidence level errors).

Our previous works clearly demonstrated that when in outburst the source emission is dominated by a soft component ($kT \sim 0.17 - 0.24$ keV) interpreted as coming from the accretion disk present around the IMBH (Godet et al. 2009; Servillat et al. 2011; Davis et al. 2011; Godet et al. 2012; Straub et al. 2014). In such a case, the decrease in the outburst duration and the average peak count rate implies that less matter is being annually accreted. In Godet et al. (2012), we stressed that the accreted mass between the outbursts in 2009 and 2010 has decreased by $\sim 46\%$. This trend continues for the outbursts in 2011 and 2012.

4. A delayed outburst

The observed evolution in the outburst duration and peak count rate may be related to a gradual decrease in the amount of mass transferred from the companion star probably leading to a decrease in the total of mass accumulated in the disk. In order to further investigate this, we proposed a monitoring of the outburst in 2013 with the *Swift*-XRT that started on 10th July 2013 and that should end at the end of 2013. Based on a recurrence period between 350 and 370 days, we expected the outburst to occur between mid-August and mid-September 2013 at the very latest. However, the X-ray outburst has been delayed by more than a month, because it started around 2nd-8th October 2013 *i.e.* MJD = 565(67 - 73). Until then, the source had remained in a low-flux state (see Fig. 1). As shown in Fig. 1, the outburst in 2013 lasted $\sim 65 - 72$ days. This strengthens the observed trend of the annual decrease in the outburst duration. The source switched to the low/hard state around 11th December 2013.

We extracted a spectrum prior to the start of the outburst *i.e.* from 19th April to 28th September 2013 (corresponding to a 38ks time exposure) and we fitted it using an absorbed powerlaw assuming an absorption column of $N_H = 4 \times 10^{20}$ cm^{-2} . We found a good fit ($C - stat/d.o.f. = 44.3/68$) with a photon index of $\Gamma = 2.5 \pm 0.6$ and a normalization of $N_\Gamma = 1.3 \pm 0.4 \times 10^{-5}$ ph $keV^{-1} cm^{-2} s^{-1}$ @ 1 keV. The derived Γ -value is consistent with the photon index found previously in the low/hard state ($\Gamma \sim 2 - 2.2$ - Servillat et al. 2011; Godet et al. 2012). The logarithm of the unabsorbed 0.2-10 keV flux is equal

to $\log F_{\text{unabs.}} = -13.11_{-0.17}^{+0.16}$. This corresponds to a luminosity of $L_X = 8.4_{-1.4}^{+1.3} \times 10^{40}$ erg cm⁻² s⁻¹. Fixing the photon index to 2.2, we found a 0.2-10 keV unabsorbed luminosity of $7.9_{-1.3}^{+1.0} \times 10^{40}$ erg s⁻¹. This X-ray luminosity appears to be larger than that derived in the low/hard state in 2009 and 2010 (see Servillat et al. 2011; Godet et al. 2012).

On MJD = 56567 (*i.e.* 2nd October 2013), we note a possible rebrightening with a 0.3-10 keV count rate of 9.6 ± 3.6 (1σ) $\times 10^{-3}$ cts s⁻¹. This data point is consistent with the count rate measured previously in the low/hard state at the 2σ level. The background subtracted spectrum reveals 5 counts in the 0.3-1.5 keV band and 5 counts in the 1.5-10 keV band. However, the following observation performed 3 days later did not show any source indicating that the flux has probably decreased again. The XRT 1.6 ks observation performed on MJD = 56573 (*i.e.* 8th October 2013) reveals a brighter X-ray source at the position of HLX-1 with a 0.3-10 keV count rate of $2.2 \pm 0.4 \times 10^{-2}$ cts s⁻¹, marking the start of the outburst in 2013. The event on MJD = 56567 may be a precursor. As opposed to previous years, we note that the peak count rate in 2013 did not decrease ($CR_{\text{peak}} = 2.5_{-0.3}^{+0.2} \times 10^{-2}$ cts s⁻¹). We extracted 2 background-subtracted spectra from 8th October 2013 to 23rd October 2013 (~ 14 ks – hereafter S1) and from 1st October 2013 to 11th December 2013 (~ 17 ks – hereafter S2). We fitted S1 using an absorbed DISKBB model, while we used an absorbed DISKBB + POWERLAW model to fit S2. Fixing the absorption column to 4×10^{20} cm⁻² and the powerlaw photon index at the best constrained value of $\Gamma = 2.2$ (see Servillat et al. 2011, Godet et al. 2012), we found a disk temperature of 0.20 ± 0.02 keV for S1 and 0.19 ± 0.03 keV for S2. The 0.2-10 keV unabsorbed luminosity was found to be $1.12_{-0.07}^{+0.06} \times 10^{42}$ erg s⁻¹ for S1 and $7.7_{-1.8}^{+0.4} \times 10^{41}$ erg s⁻¹ for S2. All these results are consistent with those obtained for previous outbursts in which the thermal component dominated the spectrum during the outburst.

5. Observational constraints put on the eccentric binary scenario

Observations of the last two (2012 & 2013) outbursts of HLX-1 provide constraints on the

eccentric-orbit donor model proposed by L11. First, the possible 1-day delay between the rise in optical and that in X-rays (Webb et al. 2014) can be explained in the framework of the mass-transfer model (MTM) only if the orbit is very nearly parabolic. The standard explanation for the long/short wavelength delay (see e.g. Pringle, Verbunt & Wade 1996) is that it is due to the density contrast propagating inwards, first through cool disk regions. The observed delay precludes a viscous propagation because, in this case, during one day the contrast would move just a couple of Schwarzschild radii at best. Assuming a propagation at the speed of sound gives an upper limit to the distance of $\sim 3 \times 10^{11}$ cm. If this is the distance where mass lost by the stellar companion is delivered to the disc, *i.e.* roughly the periastron distance, the implied eccentricity is so close to 1.0 that the orbit can be considered parabolic. This issue has been anticipated by L11 who wrote: “*the actual response of a standard accretion disk to bursts of mass transfer may be too slow to explain the observations unless the orbit is close to parabolic and/or additional heating, presumably linked to the highly time dependent gravitational potential, is invoked.*” Such a nearly parabolic, $e \rightarrow 1$, orbit can be unstable and disrupted within several orbits, as we investigate with simulations in Section 6.

The second constraint arises from the recurrence time being variable (from 350 to 370 days between 2009 and 2012) and having increased significantly in 2013. Even though the most recent outburst cycle was more than a month delayed compared to the preceding four, all the outbursts are apparently of the same type. These features can be explained in the framework of the eccentric-donor MTM only if the orbital parameters can change significantly from orbit to orbit. Indeed, such a varying orbital period is the expected behavior for certain binary systems. It is possible to either add or remove orbital energy from the system depending on the oscillation phase of the secondary at periastron, and the resulting changes in orbital period can proceed in a stochastic fashion (Mardling 1995a,b). The criterion that the evolution is stochastic is that the orbital period can change in one orbit by more than one oscillation period of the secondary (Ivanov & Papaloizou 2004, 2007).

6. Smooth Particle Hydrodynamical simulations

6.1. Numerical set-up and parameter space

To investigate this possibility for HLX-1, we use the code *Starsmasher* (Gaburov et al. 2010) to perform Newtonian smoothed particle hydrodynamical simulations of the donor initially on a parabolic incoming trajectory towards the BH. The BH is modeled as a point particle, and the donor as a polytrope with $N \approx 5 \times 10^4$ particles. We are aware that the use of less than 10^5 particles corresponds to low resolution SPH simulations. However in this work, we want to follow a large number of dynamical timescales (from 6000 to 70000) and to explore a large parameter space. This would not have been possible in large N simulations. We do investigate the effects of particle resolution on our results by varying N from 2.5×10^4 to 2×10^5 particles in one scenario. We find that the effects of using a higher particle resolution do not change the qualitative behavior of the system that we present in the following sections (see Section 6.8 for more details).

We vary the structure of the donor via the polytropic index n , and we vary the equation of state via the adiabatic index Γ . Our polytrope models are (a) $n = 1.5$, $\Gamma = 5/3$, (b) $n = 2$, $\Gamma = 1.5$, (c) $n = 2$, $\Gamma = 5/3$, and (d) $n = 3$, $\Gamma = 5/3$. By including these multiple donor models in our study, we gain a better understanding of effects due to the donor structure and equation of state. Polytrope models of type (a) above are appropriate for low mass main sequence stars, pre-main sequence stars, brown dwarfs, low-mass stripped giant cores, and low-mass white dwarfs. Polytrope models of type (d) are reasonable representations of moderately massive main-sequence stars like our Sun. Realistic models of white dwarfs with masses in the range from $0.9M_{\odot}$ to $1.3M_{\odot}$ have moments of inertia that correspond to polytropes with n between about 1.8 and 2.2 (Andronov & Yavorskij 1990); therefore polytrope types (b) and (c) provide a simple approximation for the mass distribution in moderately massive white dwarfs or stripped giant cores. Given the scale-free nature of polytropes, each simulation represents a family of cases, and we do not need to choose a physical mass or radius of the donor until after a simulation when comparisons with HLX-1 are made. We

survey parameter space by varying the mass ratio $q = M/M_{\text{BH}}$ from 10^{-3} to 10^{-5} and by varying the periapsis separation r_p from $2.2 r_t$ to $2.7 r_t$, where the tidal radius $r_t = q^{-1/3}R$ and M and R are the initial mass and radius of the donor, respectively. For fixed r_p/r_t , varying q has only a little effect beyond a rescaling of timescales, as expected for $q \ll 1$.

For convenience and computational efficiency, we use the SPH method to model only the close interactions during periapsis passages. Once the donor has retreated sufficiently far from the black hole to become stabilized (typically about 100 dynamical timescales after periapsis), we employ the analytic Kepler two-body result to advance the orbit to the same separation but now with the donor infalling toward the BH (see Antonini et al. (2011) for more details on the implementation of this method). We allow for a random fluctuation in how much time each periapsis passage is simulated, in order to randomize the oscillation phase of the secondary when it returns to periapsis and therefore to avoid the suppression of any stochastic behavior in the orbit. During this advancement of the orbit, we excise from the simulation any particles that have been stripped from the star. In this way, we are guaranteed that any changes in the orbital parameters that occur during subsequent periapsis passages are due to mass transfer and tidal effects, and not due to interactions between the donor and an under-resolved accretion disk.

If not handled carefully, artificial viscosity (AV) could spuriously damp oscillations excited in our star and spuriously transport angular momentum within it, affecting its size, structure, and rotational profile (Lombardi et al. 1999). We performed test calculations with different values of the parameters α and β used in the AV prescription described in the appendix of Ponce et al. (2012). Results of these calculations are shown in Figure 2, where we see that by decreasing the strength of the AV we better preserve the oscillations induced by the periapsis passages. Note, for example, the rather steady decrease in the amplitude of oscillations after the first periapsis passage in the $\alpha = 1$, $\beta = 2$ calculation. Given the absence of shocks in our simulations, there is no real need for AV, and we simply turn off AV completely by setting $\alpha = 0$ and $\beta = 0$ for the production runs presented in this paper. Doing so requires that

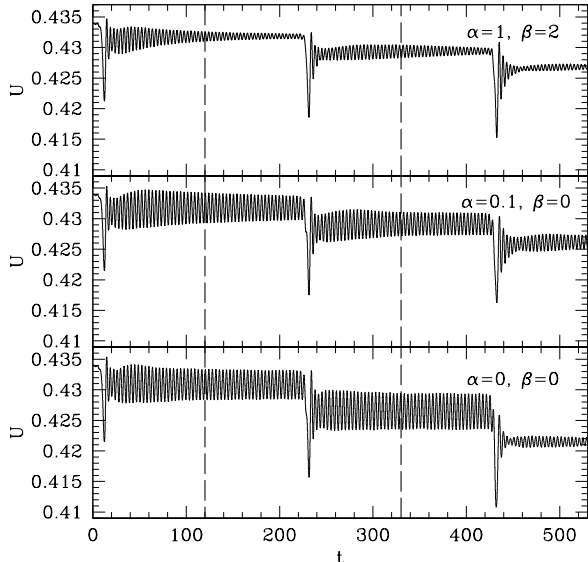


Fig. 2.— Total internal energy U versus time t for three test simulations that differ only in their artificial viscosity (AV) parameters α and β . Vertical dashed lines mark when the orbit is advanced via the Kepler two-body result. The impulse at each periastris passage (at times $t \approx 10, 220$ and 420) changes the oscillation state of the star. Local maxima in U correspond to a maximally compressed star, while local minima correspond to maximal expansion. In the top panel, stellar oscillations are quickly damped when the AV parameters $\alpha = 1$ and $\beta = 2$ are used. Oscillations are much better preserved in the $\alpha = 0.1, \beta = 0$ and especially the $\alpha = 0, \beta = 0$ simulations. The star is an $n = 1.5, \Gamma = 5/3$ polytrope, the inverse mass ratio $q^{-1} = M_{\text{BH}}/M = 3 \times 10^4$, and the initial periastris separation is $r_p = 2.3 r_t$. The unit of energy is $GM^2 R^{-1}$, while the unit of time is $(GM)^{-1/2} R^{3/2}$, where M and R are respectively the initial mass and radius of the star. The production runs in this paper use $\alpha = 0$ and $\beta = 0$.

smaller timesteps be taken, but the payoff is that the oscillation modes and rotational profile of the star are better modeled.

6.2. Evolution of the orbital parameters

We find that several of our simulations with r_p/r_t in the 2.2 to 2.7 range exhibit behavior in the pattern of orbital periods that is qualitatively consistent with that observed in HLX-1. This behavior is shown in Table 1 and Figure 3 for cases with inverse mass ratio $q^{-1} = 3 \times 10^4$. For example, notice that during periastris passages 17 through 24 of the $n = 1.5, \Gamma = 5/3, r_p = 2.4 r_t$ case (see the close-up in the bottom panel of Fig. 3), the orbital period passes through a shallow minimum, maintaining an approximate equal value for several orbits. After periastris passage 25, the orbital period increases by more than 10% (much more in this case), in qualitative accord with the recent delayed outburst of HLX-1 (see Table 1). Here, mass transfer is starting to become substantial, with slightly more mass in the tail stretching toward the black hole than in the tail extending outward. This asymmetry causes the orbit to increase in semi-major axis and eccentricity until ultimately becoming unbound, an effect previously observed in similar simulations (Faber et al. 2005, Manukian et al. 2013).

An inspection of Figure 3 reveals an even more shallow minimum in the $n = 2, \Gamma = 5/3, r_p = 2.4 r_t$ case (see the close-up in the second panel from the top in Fig. 3), with the curve actually containing two extended local minima due to the chaotic nature of the energy transfer during periastris passages (Mardling et al. 1995a,b). The emergence from these minima occur after passages 63 and 72, with a more than 10% increase in orbital period in each case. Interestingly, after the subsequent passages 64 and 73, the period decreases in one case and increases in the other. As in the corresponding $n = 1.5$ case, the system emerges from the global minimum once mass transfer becomes substantial enough to give the orbit a boost to a larger semi-major axis and eccentricity. Within several orbits, the donor becomes unbound from the BH. If a similar mechanism is indeed responsible for the orbital period variation in HLX-1, then (by definition of “stochastic”) it is not possible to predict whether the next outburst cycle will be longer or shorter than the last. However, if HLX-1 is emerging from a shallow minimum in orbital periods, the general pattern to expect would be for the duration of the outburst cycle to tend to increase until the donor is ejected

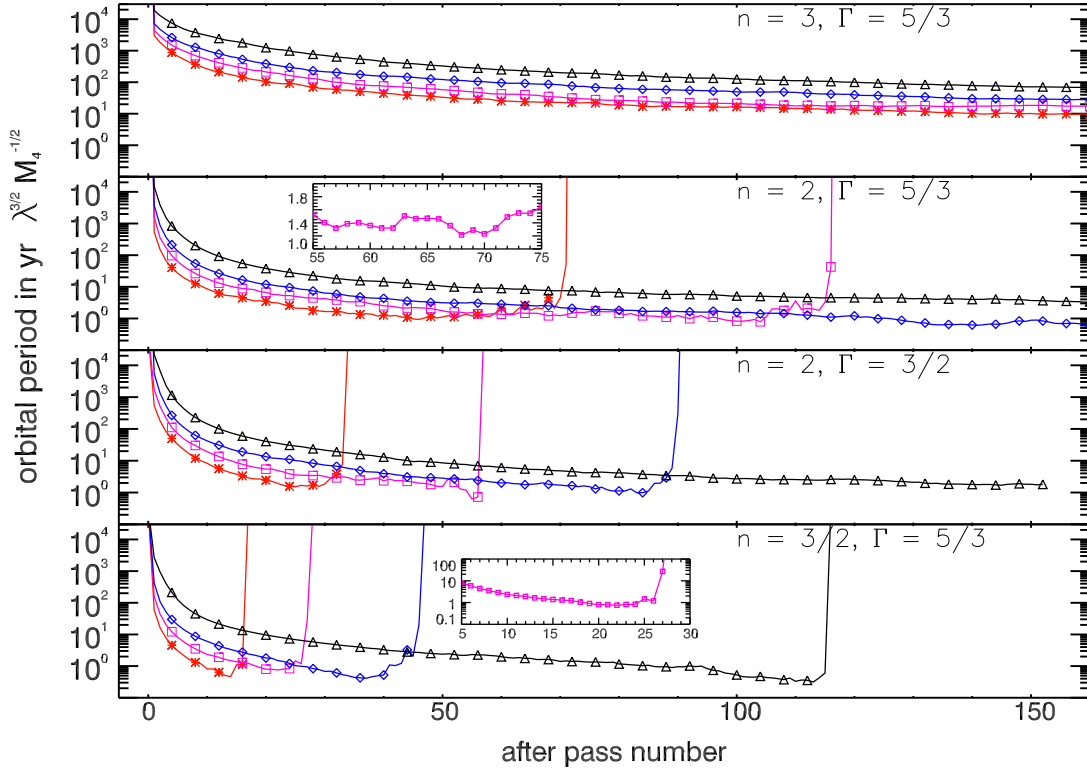


Fig. 3.— Orbital periods after periastris passages for simulations with various donor models and initial periastris separations. All donor models considered are polytropes: $n = 1.5, \Gamma = 5/3$; $n = 2, \Gamma = 1.5$; $n = 2, \Gamma = 5/3$; and $n = 3, \Gamma = 5/3$. For each type of polytrope, the results for separate initial periastris separations are shown, namely $r_p/r_t = 2.3, 2.4, 2.5$, and 2.7 (red stars, magenta squares, blue diamonds, and black triangles, respectively). Close-ups are shown for $r_p/r_t = 2.4$ for two polytropes: $n = 1.5, \Gamma = 5/3$ and $n = 2, \Gamma = 5/3$. In all cases, the inverse mass ratio $q^{-1} = 3 \times 10^4$. Curves terminate on their right edges either because the orbit becomes hyperbolic or the simulation was terminated. The units of the orbital period are $\text{yr } \lambda^{3/2} M_4^{-1/2}$, where $\lambda \equiv R/(0.01 R_\odot)$ and $M_4 \equiv M_{\text{BH}}/(10^4 M_\odot)$. Note how in the several cases, the orbital period maintains a roughly constant value of order 1 year, if $\lambda^{3/2} M_4^{-1/2} \sim 1$, before increasing.

and the mass transfer episodes stop altogether.

Periastris separations outside of the range explored in Figure 3 are interesting to consider. Situations with $r_p \gtrsim 3 r_t$ correspond to the region of parameter space explored in the classic tidal capture process (see, e.g., Novikov et al. 1992, Homan et al. 2004, Baumgardt et al. 2006). However, these situations would not provide the mass transfer events necessary to explain the quasi-periodic HLX-1 outbursts. Our simulations with $r_p \leq 2.1 r_t$ are not consistent with the observed properties of HLX-1. Although mass stripping and tidal effects during the initial periastris pas-

sage cause the orbit to become bound (while still highly eccentric), subsequent passages disrupt the donor enough to change the orbital parameters too substantially from one orbit to the next. In addition, the stochastic fluctuations are too pronounced, when compared to those seen in the cases with larger r_p .

6.3. Constraints on the donor type

To understand how our results scale with the mass ratio q , the orbital parameters after one periastris passage can be determined quasi-

analytically using the method of Press & Teukolsky (1977). For our situations, the first periapsis passage excites primarily the $l = 2$ oscillation mode of the star, and the energy transferred out of the orbit by the tidal interaction is given by

$$\Delta E = \frac{GM_{\text{BH}}^2}{R} \left(\frac{R}{r_p} \right)^6 T_2(\eta),$$

where the dimensionless function $T_2(\eta)$ is evaluated in Lee & Ostriker (1986) for three of the polytrope types considered in this paper and $\eta = (r_p/r_t)^{3/2}$. Because our initial orbit is parabolic, the semimajor axis after one passage is simply $a = GM_{\text{BH}}M/(2\Delta E)$. From Kepler's third law, the associated orbital period after the first periapsis passage is

$$P = 1.12 \times 10^{-9} \eta^6 \left(\frac{\lambda}{T_2(\eta)q} \right)^{3/2} M_4^{-1/2} \text{ yr}, \quad (1)$$

where $\lambda \equiv R/(0.01R_\odot)$ is a dimensionless measure of the donor radius and $M_4 \equiv M_{\text{BH}}/(10^4 M_\odot)$ is a measure of the black hole mass

In our simulations at a given r_p/r_t and fixed $q \ll 1$, equation (1) shows that the orbital period scales like $(R^3/(GM_{\text{BH}}))^{1/2}$. As q varies, we confirmed through simulations that the orbital periods through multiple passages scale like $q^{-3/2}$ for a given initial r_p/r_t (smaller q means larger orbits and longer orbital periods). Our results indicate that the minimum orbital period satisfies

$$P_{\text{min}} \approx p \left(\frac{\lambda}{3 \times 10^4 q} \right)^{3/2} M_4^{-1/2} \text{ yr}.$$

Here p is simply a numerical coefficient whose value depends on the type of donor and can be read off from the vertical axis of Figure 3 by looking for the minimum in the curve corresponding to the donor star under consideration. For example, for an $n = 1.5$ donor, $p \approx 0.3$ to 0.8 . For our $n = 2$ polytropes, $p \approx 0.6$ to 1.5 . In all of our simulations, p is never less than ~ 0.3 (see Fig. 3). Although prohibitive computational costs prevent us from following all curves in Figure 3 to their minima, the trends in our results are consistent with there being a minimum for any combination of donor star and initial r_p , with the value of p being more sensitive to the polytropic index n than to the adiabatic index Γ or periapsis separation

r_p . Additional test calculations done with artificial viscosity support this inference.

If the delayed outburst of HLX-1 is due to its emergence from the minimum of a curve like that shown in Figure 3, then $P_{\text{min}} \approx 1$ yr, or, after some algebraic manipulation,

$$1 \approx p \left(\frac{\lambda}{3\mu} \right)^{3/2} M_4, \quad (2)$$

where $\mu \equiv M/M_\odot$ is a dimensionless measure of the initial donor mass.

Spectral modeling and Eddington scaling from X-ray/radio data suggest that $M_{\text{BH}} \gtrsim 10^4 M_\odot$ (or equivalently $M_4 \gtrsim 1$). This then provides stringent requirements on the possible mass M and radius R of the donor. In particular, the expression on the right hand side of equation (2) is much greater than 1 for any MS star, pre-MS star, brown dwarf, or planet, ruling out the possibility of such donors in this model. The right hand side can, however, be of order unity for white dwarfs or stripped giant cores. White dwarfs obey an approximate mass-radius relation $MR^3 \approx 6 \times 10^{-7} M_\odot R_\odot^3$, or equivalently $\mu\lambda^3 \approx 0.6$, at moderate masses. Using this mass-radius relation for white dwarfs in equation (2) yields

$$M \approx 0.4 M_\odot p^{1/2} M_4^{1/2}. \quad (3)$$

A BH of mass $\sim 2 \times 10^4 M_\odot$, for example, could tidally strip matter from an $n = 1.5, \Gamma = 5/3$ WD of mass $M \sim 0.5 M_\odot$ and yield mass transfer episodes at a rate of one per year. The $n = 2$ polytropes have larger p and therefore require a larger WD mass for the same P_{min} : for example, $p \approx 1.5$ implies $M \approx 0.7 M_\odot$ for $M_4 \approx 2$. A more massive black hole would require a more massive white dwarf to achieve the same $P_{\text{min}} \approx 1$ yr.

Tidal disruption of white dwarfs by IMBHs will lead to fast rising, highly energetic events, that should be observable more often than tidal disruption of main-sequence stars (Shcherbakov et al. 2012, MacLeod et al. 2014). Simulations by Rosswog et al. (2009) of WDs and moderately massive BHs show that it is possible to trigger a nuclear explosion that would destroy the WD, as may have been the case in GRB060218 (Shcherbakov et al. 2013). However, in the simulation of Rosswog et al. (2009) that most closely resembles those presented here (see run 12 in their Table 1), the WD

is not compressed enough to trigger explosive nuclear burning.

6.4. Discussion on the mass accretion rate

Consider a system with an $M = 0.5 M_\odot$, $R = 7 \times 10^8$ cm, $n = 1.5$, $\Gamma = 5/3$ WD donor and an $M_{\text{BH}} = 2 \times 10^4 M_\odot$ BH interacting with periastris separation $r_p = 2.4 r_t = 6 \times 10^{10}$ cm (corresponding here to $\sim 10 R_g$ with R_g , the gravitational radius). In this picture, the delayed outburst of 2013 would be equated with the periastris passage represented by row 25 in Table 1, when the orbital period actually increases by substantially more than 10%. In that passage, about 2%, or $\sim 10^{-2} M_\odot$, of the mass is stripped from the WD donor. A little more than half of this stripped material falls toward the black hole: $M_{\text{fallback}} = 0.0106M = 0.0053M_\odot$. In the simulations we ran, we are unable to follow the accretion of the bound matter onto the BH. The way this matter is accreted following each periastris passage will depend on several parameters such as the BH spin, the orientation of the BH spin with respect to the system orbital plane (see e.g. Haas et al. 2012). If matter is delivered sufficiently close to the BH, general relativity effects can also become important to consider (see e.g. Dai et al. 2013).

The stripped matter has first to lose its large angular momentum before being able to be accreted by the BH. If the timescale over which most of the bound matter loses its angular momentum is sufficiently short, then a small thick accretion disk may form around the BH. Assuming that the dynamics of the stripped matter is the same as that predicted in tidal disruption events (TDEs), we estimate that the fallback time is less than ~ 1 hour using the formalism developed in Donato et al. (2014) & Rosswog et al. (2009). So, in this case a thick disk is expected to form rapidly (i.e. a few times the fallback time). Then, matter in the disk will diffuse inwards over the viscous timescale in order to be accreted by the BH. In order to have a rough estimate of the accretion rate, we use the freezing model of MacLeod et al. (2012) and Guillochon & Ramirez-Ruiz (2013) as

$$\frac{dM}{dt} = \frac{dM}{dE} \frac{dE}{dt} = \frac{1}{3} (2\pi GM_{\text{BH}})^{2/3} \frac{dM}{dE} t^{-5/3},$$

where Kepler's third law has been used to relate the specific orbital binding energy $E =$

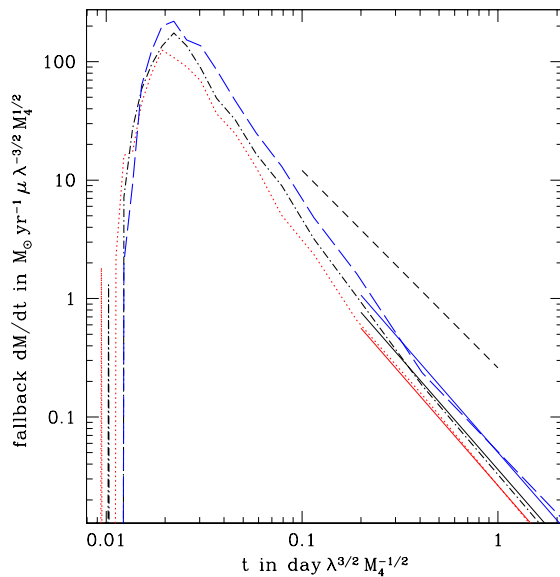


Fig. 4.— Mass fallback rate versus time after the 24th (red dotted curve), 25th (black dot-dashed curve), and 26th (blue long dashed curve) periastris passages in the $n = 1.5$, $\Gamma = 5/3$, $r_p = 2.4 r_t$ simulation. The thin solid lines at late times give the result of equation (4), with its assumed $t^{-1.9}$ dependency, for each of the passages. For comparison, the short dashed curve shows a $t^{-5/3}$ dependency. The spikes near $t = 0.01 \text{ day} \lambda^{3/2} M_4^{-1/2}$ are simply fluctuations due to single SPH particles.

$GM_{\text{BH}}/(2a)$ to the time t for material to return to periastris.²

Figure 4 shows the fallback rate dM/dt for the 24th through 26th passages. The peak fallback time is equal to $t_{\text{peak}} \sim 0.02 \text{ day} \lambda^{3/2} M_4^{-1/2}$. The peak fallback time is only weakly dependent on the donor type and on, for our close encounters, the orbital parameters. The peak fallback rate of the 25th passage, corresponding to the peak of the dot-dashed curve in Figure 4, is $(dM/dt)_{\text{peak}} = 175 \mu \lambda^{-3/2} M_4^{1/2}$ (incidentally, the coefficient of 175 is one of the entries in Table 1). For a WD orbiting in HLX-1, this corresponds to $(dM/dt)_{\text{peak}} \approx 10^2 M_\odot \text{ yr}^{-1}$, which is orders of magnitude more than the Eddington

²Note: we find the same numerical coefficient in our equation for dM/dt as in MacLeod et al. (2012), which is different than that given in Guillochon & Ramirez-Ruiz (2013).

limit, $\dot{M}_{\text{Edd}} = 2.1 \times 10^{-5} \epsilon^{-1} M_4 M_\odot \text{yr}^{-1}$ with ϵ , the radiative efficiency ($\dot{M}_{\text{Edd}} \sim 7 \times 10^{-4} M_\odot \text{yr}^{-1}$ for a $2 \times 10^4 M_\odot$ BH accreting with an efficiency of $\epsilon = \frac{1}{16}$). Our simulation results for the fallback rate at times t well after t_{peak} can be approximated as

$$\frac{dM}{dt} \approx 3.4 M_{\text{fallback}} \left(\frac{t}{\text{day} \lambda^{3/2} M_4^{-1/2}} \right)^{-1.9} \lambda^{-3/2} M_4^{1/2} \text{yr}^{-1}, \quad (4)$$

where M_{fallback} is the total mass during that periastris passage that falls back toward the BH.

From equation (4), we calculate the time t_{Edd} after a periastris passage at which the accretion drops below the Eddington accretion rate \dot{M}_{Edd} :

$$t_{\text{Edd}} \approx 550 \text{ day} \left(\epsilon \mu \frac{M_{\text{fallback}}}{M} \right)^{0.53} \lambda^{0.71} M_4^{-0.76}. \quad (5)$$

Equation (5) is used to provide the last column of information in Table 1. So, the fallback rate remains super-Eddington for only a few days. For other simulated scenarios with less fallback mass, the time until the accretion becomes sub-Eddington can be an order of magnitude smaller.

In Fig. 5, we show the fallback mass M_{fallback} and the peak fallback $(dM/dt)_{\text{peak}}$ after each periastris passage for all of the simulations presented in Fig. 3. In all cases shown in Fig. 5 and for the type of donor we consider here (a white dwarf or a stripped giant core), a brief super-Eddington accretion episode is expected to take place following the formation of a thick disk shortly after each periastris passage. Depending on the peak accretion rate, these episodes could occur within a day making the observation of such events rather challenging. The presence of powerful outflows, often invoked in the super-Eddington accretion regime (e.g. Ohsuga et al. 2005, Poutanen et al. 2007, Ohsuga & Mineshige 2011, Ohsuga & Mineshige 2013; see also De Colle et al. 2012), might make this phase even shorter by depleting matter from the disk. Such outflows coupled with the unbound stripped matter might even be able to power a nebula around the system. The t_{Edd} -values quoted in Table 1 may be considered as upper limits. Super-Eddington accretion is predicted to give rise to powerful electromagnetic emission. However, this emission may be highly anisotropic (e.g. King et al. 2001, Kawashima et al. 2012, Ohsuga & Mi-

neshige 2011, 2013). In some cases, this may even prevent observing direct emission from the inner parts of the disk if the observer line of sight is sufficiently far from the disk axis. The observed emission flux may be then significantly decreased, making the observation of such extreme events even more challenging.

Once the accretion rate is close to or below the critical value, most of the outflows might switch off (except maybe within the innermost parts of the disk), making possible the direct observation of the disk emission. This would lead to a rapid increase in the source luminosity in X-rays and optical. In such a picture, the super-Eddington accretion episodes would appear as precursors to the main outbursts that would correspond to matter accreted at a rate close to or below the Eddington limit. We did not find any strong evidence in the observational data collected so far for the presence of a precursor preceding the main outburst. However, this can be easily accounted for in our observing strategy to monitor the change in luminosity in HLX-1, since the shortest timescale used when the source was in the low/hard state was to collect a 1 ks snapshot every 2 days.

In Fig. 5, the general pattern is that the peak fallback rate tends to increase over several periastris passages, even if from passage to passage the value of the accretion rate could vary in a stochastic manner due to the effects of stochastic fluctuations on the star (see Section 6.6). Even if this seems to be difficult to reconcile with our observations, how this translates in term of outburst duration deserves a proper investigation that is beyond the scope of the present paper. Another important point to consider in future works is that in the case of HLX-1 we know from the X-ray observations that there is still some material accreted when the source is in the low/hard state. How this material and the matter transferred from the star at periastris interact to give rise to an accretion disk around the BH also deserves detailed scrutiny.

6.5. Discussion on the lifetime of such a highly eccentric system

Figure 6 shows the lifetime of the system (Δt_{sys}) for the different cases shown in Figure 3. The lifetime of the system strongly depends on how efficient is the tidal stripping of the donor star. Thus, the distance at periastris and the com-

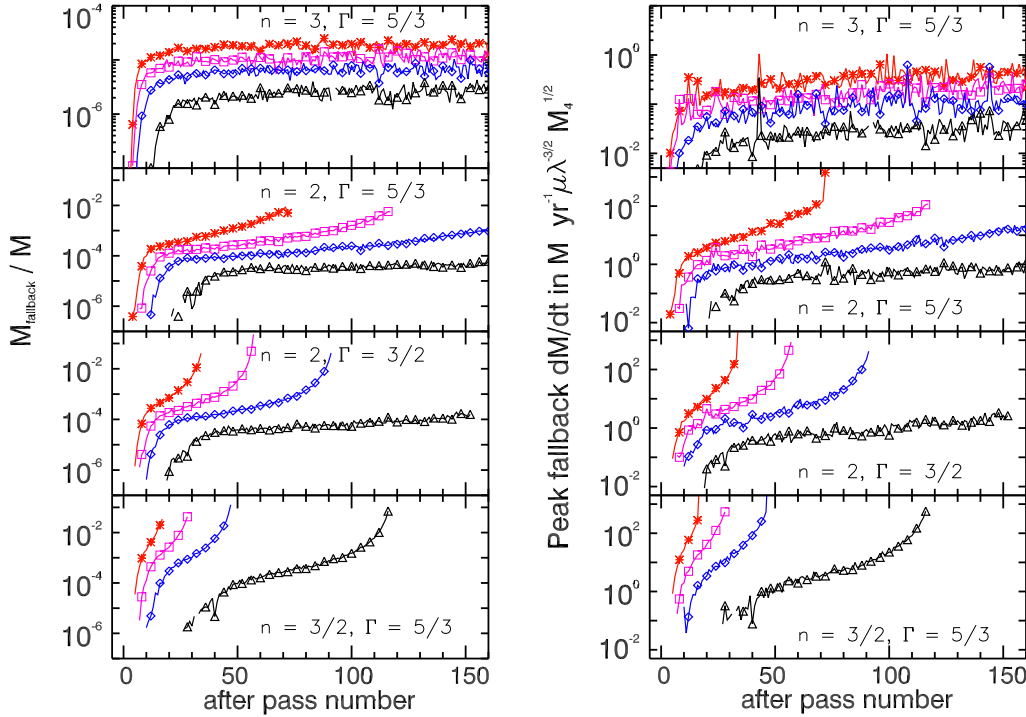


Fig. 5.— *Left* – Ratio of the fallback mass over the donor mass; *Right* – the peak fallback rate $(dM/dt)_{\text{peak}}$. Data point types are as in Fig. 3.

position of the donor star (i.e. the equation of state of the polytrope considered) have a significant impact on Δt_{sys} . Smaller r_p/r_t -values imply that more matter is transferred towards the BH at a given periapsis passage (see Fig. 5). This results in a quicker way to make the star unbound to the BH (see Section 6.6). In all cases considered in this paper, the Δt_{sys} -values appear to be rather short. For the case of the WD donor around a $2 \times 10^4 M_{\odot}$ BH considered in the above sections (i.e. $r_p/r_t = 2.4$, $\lambda = 1$, $n = 1.5$ & $\Gamma = 5/3$), $\Delta t_{\text{sys}} \sim 220$ years; which makes the detection of such a system very challenging. Note the lifetime of the system will even be smaller when considering higher BH mass since $\Delta t_{\text{sys}} \propto M_{\text{BH}}^{-1/2}$.

Obviously, the lifetime of the system is not related to the time interval over which the source emission will be detectable. The latter time depends on when mass transfer starts and how much matter remains in the disk before the star is ejected. As seen in Fig. 5 (black triangles i.e.

$r_p/r_t = 2.7$), mass transfer episodes do not necessarily start once the star becomes bound to the BH. During the first periapsis passages, the star radius is too small for mass transfer to take place. Once the star radius increases enough due to the star oscillations induced by tidal forces over successive periapsis passages, mass transfer episodes will start. When mass transfer episodes stop because the star has been ejected, the source should stay in the low/hard state until the source will run out of fuel. Once this happens, then the source will switch into quiescence. According to this scenario, when the donor star will be ejected, HLX-1 should look like a moderately bright ULX in the outskirts of the ESO 243-49 S0 galaxy with an X-ray luminosity of $\sim 10^{40}$ erg s^{-1} displaying spectral properties consistent with some known ULXs.

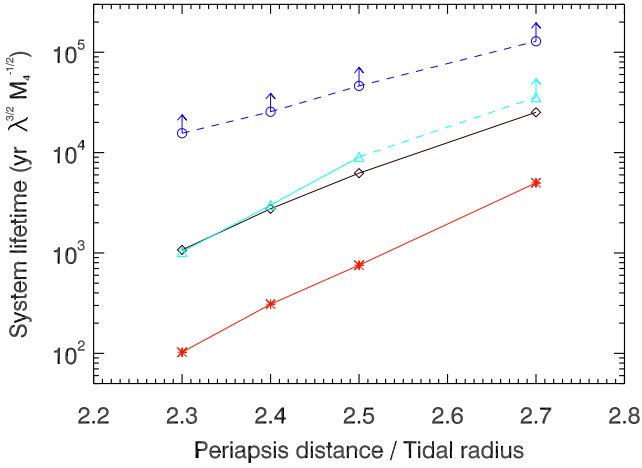


Fig. 6.— Lifetime of the system for the different cases shown in Figure 3: $n = 1.5, \Gamma = 5/3$ (red stars), $n = 2, \Gamma = 5/3$ (black squares), $n = 2, \Gamma = 1.5$ (cyan triangles) and $n = 3, \Gamma = 5/3$ (blue circles). The data points for which the simulation was stopped before the star becomes unbound to the BH because of too prohibitive computation time are marked with vertical arrows. Therefore, they correspond to lower limits on the lifetime of the system.

6.6. Discussion on the stochastic orbital evolution

Our simulations suggest the pattern in orbital period and outbursts in HLX-1 could be explained by the combination of mass transfer and stochastic orbital evolution. This is illustrated in Figure 7 comparing the evolution over time of the changes in orbital period from one orbit to the next (dP) and the fraction of mass falling onto the BH (F_{bound}). The curves are shown for the case: $r_p/r_t = 2.5$, $n = 1.5$ & $\Gamma = 5/3$ with artificial viscosity turned off. The passages with $F_{\text{bound}} > 50\%$ of the mass falling onto the black hole result in a smaller decrease in orbital period than for those passages with $F_{\text{bound}} \leq 50\%$. This could be understood as mass loss falling onto the BH “pushes” the orbit to larger semimajor axis, while mass loss towards infinity “pushes” the orbit to smaller semimajor axis. Similar behavior is seen for the other cases considered in this paper. It appears that stochastic behavior in mass loss is tied to stochastic behavior in the orbital period.

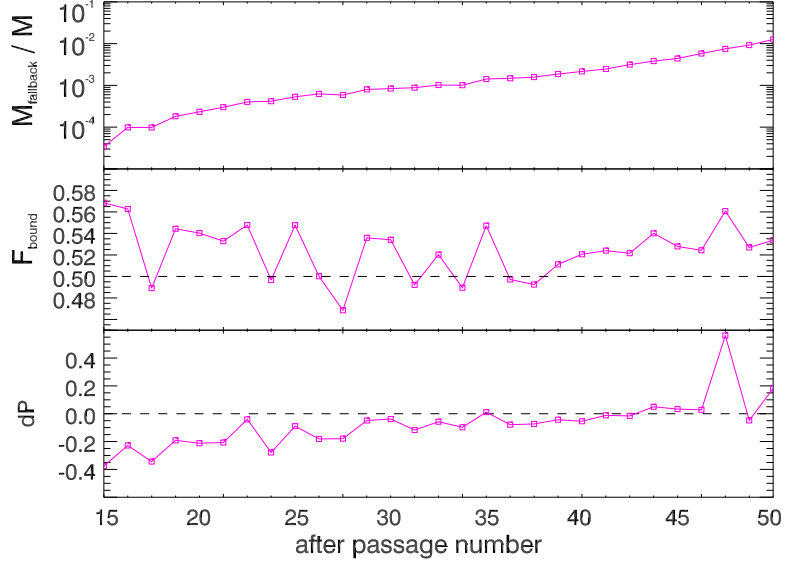


Fig. 7.— Effects of stochastic fluctuations on the orbital evolution. Top – Ratio of the fallback mass to the initial mass of the star; Middle – Fraction of the stripped matter bound to the BH; Bottom – change in the orbital period from one orbit to the next. The three curves are shown for the case: $r_p/r_t = 2.5$, $n = 1.5$ & $\Gamma = 5/3$ with artificial viscosity turned off. dP is given in units of $\text{yr } \lambda^{3/2} M_4^{-1/2}$.

The appearance of stochastic behavior in mass loss are due to the development of stochastic fluctuations inside the star. For most cases considered here, the criterion for stochastic fluctuations is satisfied from the first orbits; which means that the phase of the oscillation is essentially randomized at the next periapsis passage. Most orbital energy gets dumped into the $l = 2$ mode of oscillation. This does not imply that stochastic fluctuations will necessarily have large effects on the behavior of the orbital period at early times. Once the star is sufficiently perturbed after several periapsis passages, the randomness of the oscillation phase at periapsis results in a randomness in which sides the star will be bulged out at periapsis, and therefore the amount of mass stripping will depend on which way the star happens to be bulging at periapsis. When the amount of mass stripping becomes substantial at later times, this could lead to large positive changes in the orbital period, mak-

ing the system less bound and ultimately the star will be ejected.

If the energy is dumped into many modes of oscillation, then the stochastic effects on the orbit are diminished (e.g. Kochanek 1992). Each mode of oscillation has its own oscillation period, and whether there is energy put into the orbit or taken out of the orbit, from one particular mode, depends on the relative phase of the oscillation and the orbit at periapsis. If there are many modes of oscillation that have been excited, then some of the modes will remove energy from the orbit, while other modes will add energy to the orbit, and these effects tend to cancel so that the stochastic behavior is less evident. If there are only a small number of modes that are substantially excited, then the stochastic behavior is more evident because when adding up the individual effects there are too few of them always to get an overall cancellation.

Below, we apply the equations of Ivanov & Papaloizou (2007, hereafter IP) to understand better under what conditions the stochastic process can give the necessary orbital period fluctuations.³ We calculate the minimum separation at which the stochastic instability would operate from equation (13) of IP:

$$a_{\text{st}} \approx \lambda \mu^{-3/5} M_4^{3/5} (\Delta \tilde{E})^{-2/5} 10^{11} \text{cm},$$

where the fractional change in orbital binding energy $\Delta \tilde{E} \equiv \Delta E/E$ can be calculated from equation (7) in IP and the specific orbital binding energy $E = GM_{\text{BH}}/(2a)$. Here we neglect the contribution of gravity waves to $\Delta \tilde{E}$, which have a secondary effect on the orbital evolution, at least for slowly rotating white dwarfs (see the discussion in IP at the end of their §4).

³It is worth noting that the theory of linear tides presented in IP is not intended to be applied once mass transfer and mass loss occur. Still, the criterion for stochastic behavior can be expressed as the number of oscillations that the donor undergoes between periapsis passages changing by more than 1 from one orbit to the next. This condition can equivalently be expressed as the phase change $\delta\Phi > 2\pi$, so that phase coherence is lost and the donor is in an essentially random phase with each successive orbit. Mass transfer and mass loss alter not only the orbital period P_{orb} but also the fundamental oscillation frequency ω_f of the donor, so that $\delta\Phi = \omega_f \delta P_{\text{orb}} + P_{\text{orb}} \delta\omega_f$. While $\delta\omega_f = 0$ in the scenario treated by IP, here the non-zero $\delta\omega_f$ acts to make the region of parameter space within which stochastic behavior operates even larger than what the equations of IP imply.

For instance, consider a donor star orbiting a BH with a 1 yr orbital period, as in our model for HLX-1. By Kepler's third law, the semimajor axis $a = 3.2 \times 10^{14} \text{cm} M_4^{1/3}$. For a WD secondary that satisfies the mass radius relation $\mu\lambda^3 \approx 0.6$ and that has a mass given by equation (3) with $p \sim 1$, the condition $a > a_{\text{st}}$ requires roughly $\Delta \tilde{E} \gtrsim 10^{-8} M_4^{-1/2}$. We find for our WD that $\Delta \tilde{E} \approx 20/(\phi\Psi)$, where ϕ is a function of $\eta \equiv (r_p/r_t)^{3/2}$ given by equation (8) of IP and Ψ is a rotation parameter given by their equation (12). For $M_4 \sim 2$ and a non-rotating star ($\Psi = 1$), the condition $a > a_{\text{st}}$ requires $\eta \equiv (r_p/r_t)^{3/2} \lesssim 9$ or $r_p/r_t \lesssim 4.3$. For $M_4 \sim 2$ and a star rotating near breakup, $\Delta \tilde{E} \gtrsim 10^{-8} M_4^{-1/2}$ requires $\eta \lesssim 7$ or equivalently $r_p/r_t \lesssim 3.7$. We therefore should expect stochastic behavior in all of our scenarios we are considering.

Should the stochastic fluctuations be large enough to explain a $\sim 10\%$ change in orbital period? A 10% change in period requires a $\sim 7\%$ change in semimajor axis or in orbital energy: $0.07 \approx \Delta \tilde{E}$.

So, for a slowly rotating WD, a $\sim 10\%$ change in period requires $\phi \sim 300$, which corresponds to $\eta \sim 3.5$ or $r_p/r_t \sim 2.3$. We note that this rough estimate neglects orbital energy changes associated with mass loss, so we expect 10% fluctuations in orbital period also to be obtainable in scenarios that had initial r_p/r_t larger than 2.3. As found in our simulations, the stochastic fluctuations in orbits with initial r_p/r_t in the 2.3 to 2.7 range are the right order of magnitude to explain what is being observed in HLX-1. Although computational costs prohibit us from following situations with initial $r_p/r_t > 2.7$ all the way down to the minimum in orbital period, such scenarios may also provide large enough stochastic fluctuations to explain the behavior of HLX-1.

6.7. Effects of viscosity on the orbital period

We ran all our simulations with AV turned off. As shown in Fig. 2, the effects of viscosity are to damp the tidal oscillations of the star so that the effects of stochastic fluctuations are mostly suppressed. This results in a smoother behavior in mass loss and hence smoother changes in the orbital period as seen in Figure 8. Due to the al-

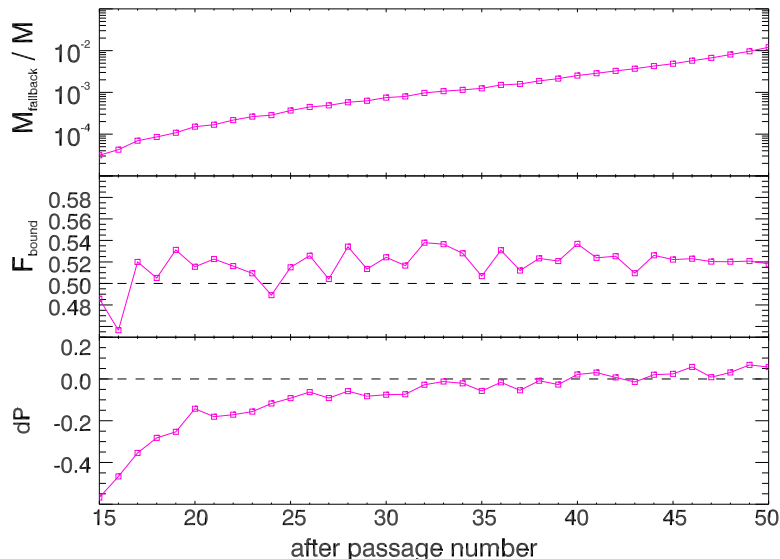


Fig. 8.— Same legend as in Fig. 7, but with artificial viscosity turned on ($\alpha = 1$ & $\beta = 2$).

most complete suppression of stochastic fluctuations, the star will stay bound to the BH on a longer timescale than in the case without AV (see Fig. 9). However, the star is expected to be ultimately ejected with and without AV. We note that at later times when the star is heavily perturbed stochastic behavior in the orbital period could be observed in the simulations we ran with AV turned on.

Do the effects of viscosity play an important role in damping the star oscillations in the case where the donor is a white dwarf?

Kochanek (1992) stressed that viscosity can damp the oscillations of a star and suppress stochastic effects. The Q value is a measure of how many oscillations there are before there is substantial damping of a mode. Therefore, with the period of the oscillation mode scaling (ν_{mode}) with the dynamical timescale, the effects of viscosity can be neglected if:

$$\nu_{\text{mode}} = \left(\frac{R^3}{\sqrt{GM}} \right) \times Q > \sim P$$

with P being the orbital period. For $P \sim 1$ year, this inequality is not satisfied for main sequence stars with $Q < \sim 10^6$. However, Piro (2011) invokes higher Q -values for WDs in his work on WD

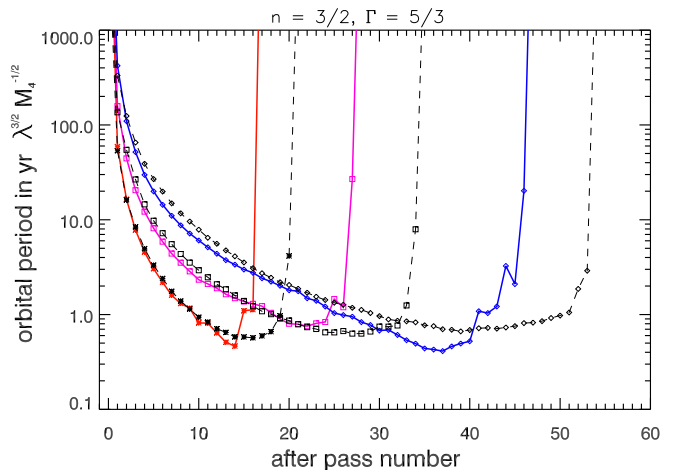


Fig. 9.— Effects of viscosity on the evolution of the orbital period for the case: $n = 1.5$ & $\Gamma = 5/3$ and different r_p/r_t values: 2.3 (red stars), 2.4 (magenta squares) and 2.5 (blue diamonds). Thick lines correspond to simulations run with AV turned off and dashed lines correspond to simulations run with AV turned on.

binaries. He found $Q = 7 \times 10^{10}$ and $Q = 2 \times 10^7$, respectively for He and C/O WDs. The above inequality is easily satisfied if we use $Q = 7 \times 10^{10}$, while it is barely satisfied for $Q = 2 \times 10^7$. However, as stressed by Piro (2011) the appropriate range of Q -values is still unknown for WDs. Some authors have estimated Q -values up to 10^{12} (e.g. Campbell 1984) or 10^{15} (Willems et al. 2010).

6.8. Effects of particle resolution

Fig. 10 shows the effects of particle resolution (N) on the evolution of the orbital period, the ratio of the fallback mass to the initial mass of the donor, the fraction of the stripped matter bound to the BH (F_{bound}) and the change in the orbital period from one orbit to the next (dP) for the case with $r_p/r_t = 2.3$, $n = 1.5$ & $\Gamma = 5/3$. In all cases, the inverse mass ratio $q^{-1} = 3 \times 10^4$. Here we considered N -values varying from 2.5×10^4 to 2×10^5 particles. From this figure, we can see that overall the higher resolution simulations behave qualitatively the same way as for lower resolution cases presented in previous sections. Indeed, the donor is ejected from the system at passage 17 whatever the particle resolution used. We note

that mass stripping appears to begin sooner as N increases, while dP and F_{bound} appear to vary more smoothly at our highest resolution ($N = 2 \times 10^5$ particles). Even so, there still is a significant change in orbital period between two successive passages in this latter case. So, we are confident that the results discussed on this paper are robust.

7. Conclusion

After showing quasi-periodic outbursts in HLX-1 over the past four years, the X-ray outburst in 2013 was delayed by more than a month. In this paper, we investigated the implications of this delay in the framework of the mass transfer model proposed by L11 and the orbital constraints derived from Webb et al. (2014). To do so, we performed Newtonian SPH simulations over a large parameter space for the donor type using polytropes with various equations of state and the orbital parameters in order to study several points: 1) Could the orbital parameters change suddenly in such a way to explain the delayed outburst?; 2) Could an IMBH capture a star without disrupting it on a nearly parabolic bound orbit? What will be the fate of such a system? In a forthcoming paper, we will calculate the probability to form such highly eccentric systems and estimate the space density of such systems in the local Universe; 3) Could we put some constraints on the possible type of donor stars?

Our results show that an incoming star approaching a BH on a parabolic orbit could become bound to the BH with an orbital eccentricity close to 1. After the formation of such a highly elliptical binary system, the orbital period will decrease until reaching a minimum that can be shallow. Then, the orbital period will tend to generally increase over several periapsis passages due to tidal effects and increasing mass transfer. This will ultimately end with the star being ejected. Depending on the reservoir of matter remaining in the accretion disk, the BH will continue accreting this matter over a timescale that could be much larger than the time during which the star was bound to the BH. The source will then stay in the low/hard state and will appear as a moderately bright ULX ($L_X \sim 10^{40}$ erg s $^{-1}$) until switching to quiescence when running out of fuel.

In the cases matching the behavior of HLX-1,

our simulations showed that the donor star could perform several orbits before the system is disrupted in qualitative agreement with our current observations. We also demonstrated the importance of the effects of stochastic fluctuations inside the star that appear to be tied to stochastic behavior in mass loss and that, by adding or removing orbital energy from the system, could lead to sudden changes in the orbital period from one periapsis passage to the next with the appropriate order of magnitude of what has been observed for HLX-1.

Given the constraints on the BH mass ($M_{\text{BH}} > 10^4 M_{\odot}$) and assuming that the HLX-1 system is currently near a minimum in orbital period, a recurrence time around 1 year implies that the donor star has to be a WD or a stripped giant core passing at periapsis at only a few gravitational radii from the IMBH. We also discussed the possibility that given the substantial amount of matter transferred at periapsis this might give rise to an extreme and brief supercritical accretion episode. Although spectral fitting of the X-ray data do not favor supercritical accretion, we speculate that such high accretion episodes might be missed by observations not done within a fraction of a day preceding the start of the outburst. So, the increase in mass transferred to the accretion disk at each periapsis is an important process to consider in more detail and possibly the biggest challenge to the MTM presented in this paper.

We would like to thank J.-P. Lasota, G. Dubus & A. King for useful discussions. We thank the anonymous referee for his/her comments. JCL is supported by National Science Foundation (NSF) Grant No. AST-1313091. This work used the Extreme Science and Engineering Discovery Environment (XSEDE), which is supported by NSF grant number OCI-1053575.

Facilities: Swift.

REFERENCES

- Alexander, D. M. & Hickox, R. C. 2012, *New Astronomy Reviews*, 56, 93
- Andronov, I. L., & Yavorskij, Y. B. 1990, *Contributions of the Astronomical Observatory Skalnaté Pleso*, 20, 155

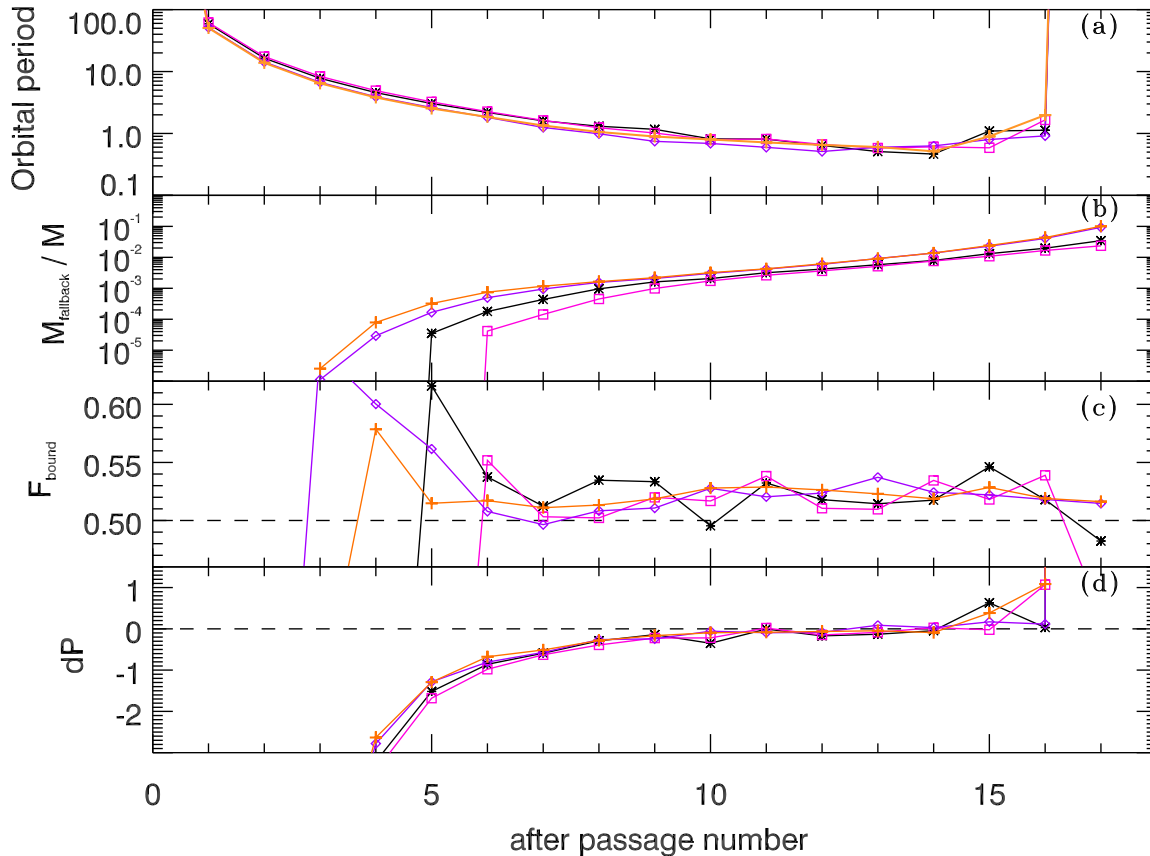


Fig. 10.— Effects of the particle resolution N for the case with $n = 1.5$ & $\Gamma = 5/3$ & $r_p/r_t = 2.3$ on the evolution of the orbital period (a), the ratio of the fallback mass to the initial mass of the donor (b), the fraction of the stripped matter bound to the BH (c) and the change in the orbital period from one orbit to the next (d). In all cases, the inverse mass ratio $q^{-1} = 3 \times 10^4$. The symbols correspond to squares for $N = 2.5 \times 10^4$, stars for $N = 5 \times 10^4$, diamonds for $N = 10^5$ and crosses for $N = 2 \times 10^5$, respectively. The epoch when mass stripping starts happens earlier with higher particle resolution. Indeed, mass stripping starts at passage 6 for $N = 2.5 \times 10^4$, while for $N = 1 - 2 \times 10^5$ it starts at passage 3.

Antonini, F., Lombardi, J. C., Jr., & Merritt, D. 2011, *ApJ*, 731, 128

Arnaud, K., 1996, in Jacoby G. Barnes., eds, *Astronomical Data Analysis Software and Systems*, ASP Conf. Series, 101, 17

Baumgardt, H., Hopman, C., Portegies Zwart, S., & Makino, J. 2006, *MNRAS*, 372, 467

Burrows, D. N. et al. 2005, *Space Sci. Rev.*, 120, 165

Campbell, C. G. 1984, *MNRAS*, 207, 433

Cash, W. 1979, *ApJ*, 228, 939

Davis, S. W. et al. 2011, *ApJ*, 734, 111

De Colle, F., Guillochon, J., Naiman, J., & Ramirez-Ruiz, E. 2012, *ApJ*, 760, 103

Dai, L., Escala, A. & Coppi, P. 2013, *ApJ*, 775, L9

Donato, D. et al. 2014, *ApJ*, 781, 13

Evans, P. A. et al. 2009, *MNRAS*, 397, 1177

Faber, J. A., Rasio, F. A., & Willems, B. 2005, *Icarus*, 175, 248

Farrell, S. A., Webb, N. A., Barret, D., Godet, O. & Rodrigues, J. M. 2009, *Nature*, 460, 73

- Feng, H. & Soria, R. 2011, *New Astronomy Reviews*, 55, 166
- Gaburov, E., Lombardi, J. C., Jr., & Portegies Zwart, S. 2010, *MNRAS*, 402, 105
- Gehrels, N. et al. 2004, *ApJ*, 611, 1005
- Godet, O. et al. 2009, *ApJL*, 705, 109
- Godet, O. et al. 2012, *ApJ*, 752, 34
- Greene, J. E. & Ho, L. C. 2004, *ApJ*, 610, 722
- Guillochon, J., & Ramirez-Ruiz, E. 2013, *ApJ*, 767, 25
- Haas, R., Shcherbakov, R. V., Bode, T. & Laguna, P. 2012, *ApJ*, 749, 117
- Hopman, C., Portegies Zwart, S. F., & Alexander, T. 2004, *ApJ*, 604, L101
- Ivanov, P. B., & Papaloizou, J. C. B. 2004, *MNRAS*, 347, 437
- Ivanov, P. B., & Papaloizou, J. C. B. 2007, *A&A*, 476, 121
- Kalberla, P. M. W., Burton, W. B., Hartmann, D. et al. 2005, *A&A*, 440, 775
- Kawaguchi, T. 2003, *ApJ*, 593, 69
- Kawaguchi, T., Aoki, K., Ohta, K., Collin, S. 2004, *A&A*, 420, L20
- Kawashima, T. et al. 2012, *ApJ*, 152, 18
- King, A. R. et al. 2001, *ApJ*, 552, 109
- King, A. R. & Lasota, J.-P. 2014, accepted for publication in *MNRAS*, arXiv:1407.0557
- Kochanek, C. S. 1992, *ApJ*, 385, 604
- Lasota, J.-P. 2001, *New. A. Rev.*, 45, 449
- Lasota, J.-P. et al. 2011, *ApJ*, 735, 89
- Lee, H. M., & Ostriker, J. P. 1986, *ApJ*, 310, 176
- Lombardi, J. C., Sills, A., Rasio, F. A., & Shapiro, S. L. 1999, *Journal of Computational Physics*, 152, 687
- MacLeod, M., Guillochon, J., & Ramirez-Ruiz, E. 2012, *ApJ*, 757, 134
- MacLeod, M., Goldstein, J., Ramirez-Ruiz, E., Guillochon, J., & Samsing, J. 2014, *ApJ*, 757, 134
- Madau, P., Rees, M.J. 2001, *ApJL*, 551, L27
- Manukian, H., Guillochon, J., Ramirez-Ruiz, E., & O'Leary, R. M. 2013, *ApJ*, 771, L28
- Mardling, R. A. 1995a, *ApJ*, 450, 722
- Mardling, R. A. 1995b, *ApJ*, 450, 732
- Miller, M. C. & Colbert, E. J. M. 2004, *International Journal of Modern Physics D*, 13, 1
- Miller, M. C., Farrell S. A. & Maccarone, T. J. 2014, *ApJ*, 788, 116
- Novikov, I. D., Pethick, C. J., & Polnarev, A. G. 1992, *MNRAS*, 255, 276
- Ohsuga, K., Mori, M., Nakamoto, T., Mineshige, S. 2005, *ApJ*, 628, 368
- Ohsuga, K. & Mineshige, S. 2011, *ApJ*, 736, 2
- Ohsuga, K. & Mineshige, S. 2013, *Space Science Reviews*, DOI 10.1007/s11214-013-0017-3
- Piro, A. L. 2011, *ApJ*, 740, 53L
- Ponce, M., Faber, J. A., & Lombardi, J. C. 2012, *ApJ*, 745, 71
- Pooley, D., & Rappaport, S. 2006, *ApJL*, 644, L45
- Poutanen, J. et al. 2007, *MNRAS*, 377, 1187
- Press, W. H., & Teukolsky, S. A. 1977, *ApJ*, 213, 183
- Pringle, J. E., Verbunt, F., & Wade, R. A. 1986, *MNRAS*, 221, 169
- Remillard, R. A. & McClintok, J. E. 2006, *ARA&A*, 44, 49
- Roberts, T. P. 2007, *ApSS*, 311, 203
- Rosswog, S., Ramirez-Ruiz, E., & Hix, W. R. 2009, *ApJ*, 695, 404
- Shcherbakov, R. V., Pe'er, A., Reynolds, C. S., et al. 2012, *European Physical Journal Web of Conferences*, 39, 2007

Shcherbakov, R. V., Pe'er, A., Reynolds, C. S., et al. 2013, ApJ, 769, 85

Servillat, M. et al. 2011, ApJ, 743, 6

Soria, R., Hau, G. K. T. & Pakull, M. W. 2013, ApJL, 768, L22

Strader, J. et al. 2012, ApJL, 750, L27

Straub, O., Godet, O., Servillat, M., Barret, D. & Webb, N. A., 2014, submitted to A&A, arXiv:1403.6407

Webb, N. A. et al. 2010, ApJ, 712, 107

Webb, N. A. et al. 2012, Science, 337, 554

Webb, N. A. et al. 2014, ApJL, 780, 9

Wiersema et al. 2010, ApJ, 721, 102

Willems, B., Deloye, C. J., & Kalogera, V. 2010, ApJ, 713, 239

TABLE 1
RESPONSE OF ORBITAL PARAMETERS AND MASS LOSS TO MULTIPLE PERIAPSIS PASSAGES.

after passage number	orbital period	semimajor axis a/R	eccentricity	M_{donor}/M	peak fallback dM/dt	M_{fallback}/M	t_{Edd}
$n = 1.5, \Gamma = 5/3, r_p = 2.4r_t$							
1	158.	0.135E+08	0.99999	1.0000	0.0	0.0	0.0
2	44.4	0.581E+07	0.99999	1.0000	0.0	0.0	0.0
3	20.5	0.347E+07	0.99998	1.0000	0.0	0.0	0.0
4	12.2	0.245E+07	0.99997	1.0000	0.0	0.0	0.0
5	8.13	0.187E+07	0.99996	1.0000	0.0	0.0	0.0
6	5.87	0.151E+07	0.99995	1.0000	0.0	0.0	0.0
7	4.40	0.124E+07	0.99994	0.99999	0.17	0.33E-05	0.20
8	3.52	0.107E+07	0.99993	0.99995	0.56	0.28E-04	0.63
9	2.85	0.932E+06	0.99992	0.99981	1.7	0.77E-04	1.1
10	2.33	0.814E+06	0.99991	0.99957	2.0	0.13E-03	1.4
11	2.11	0.761E+06	0.99990	0.99909	4.3	0.28E-03	2.1
12	1.90	0.709E+06	0.99989	0.99832	4.9	0.44E-03	2.7
13	1.64	0.644E+06	0.99988	0.99714	7.0	0.64E-03	3.3
14	1.49	0.604E+06	0.99988	0.99549	10.6	0.891E-03	3.9
15	1.37	0.572E+06	0.99987	0.99334	13.8	0.113E-02	4.5
16	1.30	0.551E+06	0.99986	0.99097	18.0	0.128E-02	4.7
17	1.23	0.531E+06	0.99986	0.98801	20.6	0.156E-02	5.3
18	1.04	0.476E+06	0.99984	0.98421	26.3	0.196E-02	6.0
19	0.898	0.431E+06	0.99983	0.97979	29.1	0.226E-02	6.4
20	0.799	0.399E+06	0.99981	0.97476	41.5	0.264E-02	7.0
21	0.792	0.396E+06	0.99981	0.96800	54.5	0.358E-02	8.2
22	0.754	0.384E+06	0.99981	0.95963	60.0	0.441E-02	9.2
23	0.808	0.402E+06	0.99981	0.94907	84.3	0.552E-02	10.
24	0.834	0.410E+06	0.99982	0.93418	125.	0.776E-02	12.
25	1.46	0.595E+06	0.99987	0.91431	175.	0.106E-01	15.
26	1.19	0.521E+06	0.99986	0.88596	220.	0.147E-01	17.
27	26.9	0.416E+07	0.99998	0.84008	350.	0.243E-01	23.
28	Infinity	-0.370E+07	1.0000	0.75818	544.	0.424E-01	30.
$n = 2, \Gamma = 1.5, r_p = 2.3r_t$							
26	1.68	0.653E+06	0.99989	0.97546	25.5	0.183E-02	5.7
27	1.60	0.633E+06	0.99989	0.97110	34.4	0.231E-02	6.5
28	1.71	0.662E+06	0.99989	0.96559	43.2	0.296E-02	7.4
29	1.56	0.623E+06	0.99989	0.95839	54.0	0.372E-02	8.4
30	1.87	0.703E+06	0.99990	0.94886	71.2	0.502E-02	9.8
31	2.84	0.928E+06	0.99992	0.93506	103.	0.738E-02	12.

TABLE 1—Continued

after passage number	orbital period	semimajor axis a/R	eccentricity	M_{donor}/M	peak fallback dM/dt	M_{fallback}/M	t_{Edd}
$n = 2, \Gamma = 5/3, r_p = 2.3r_t$							
50	1.12	0.498E+06	0.99986	0.95619	23.8	0.136E-02	4.9
51	1.22	0.529E+06	0.99986	0.95378	23.8	0.132E-02	4.8
52	1.12	0.499E+06	0.99986	0.95099	24.5	0.143E-02	5.0
53	1.18	0.517E+06	0.99986	0.94800	32.9	0.160E-02	5.4
54	1.37	0.571E+06	0.99987	0.94486	37.9	0.169E-02	5.5
55	1.20	0.523E+06	0.99986	0.94153	31.6	0.171E-02	5.5
$n = 2, \Gamma = 5/3, r_p = 2.4r_t$							
56	1.40	0.581E+06	0.99987	0.98405	4.6	0.29E-03	2.2
57	1.32	0.557E+06	0.99987	0.98341	5.1	0.30E-03	2.2
58	1.39	0.576E+06	0.99987	0.98282	5.7	0.35E-03	2.4
59	1.40	0.580E+06	0.99987	0.98219	6.6	0.35E-03	2.4
60	1.36	0.568E+06	0.99987	0.98145	6.4	0.38E-03	2.5
61	1.32	0.557E+06	0.99987	0.98076	6.9	0.35E-03	2.4
62	1.32	0.557E+06	0.99987	0.98006	6.1	0.38E-03	2.5
63	1.51	0.608E+06	0.99988	0.97928	8.1	0.46E-03	2.8
64	1.46	0.597E+06	0.99988	0.97848	7.6	0.40E-03	2.6
...							
68	1.21	0.527E+06	0.99986	0.97521	8.0	0.37E-03	2.5
69	1.29	0.549E+06	0.99986	0.97437	8.8	0.48E-03	2.8
70	1.23	0.532E+06	0.99986	0.97350	6.4	0.45E-03	2.7
71	1.32	0.557E+06	0.99987	0.97243	8.9	0.61E-03	3.2
72	1.49	0.604E+06	0.99988	0.97160	8.2	0.51E-03	2.9
73	1.55	0.620E+06	0.99988	0.97052	9.6	0.61E-03	3.2
$n = 2, \Gamma = 5/3, r_p = 2.5r_t$							
143	0.671	0.355E+06	0.99978	0.95006	13.1	0.621E-03	3.2
144	0.658	0.350E+06	0.99978	0.94879	11.4	0.666E-03	3.4
145	0.670	0.354E+06	0.99978	0.94769	13.2	0.580E-03	3.1
146	0.717	0.371E+06	0.99979	0.94640	13.3	0.747E-03	3.6
147	0.809	0.402E+06	0.99981	0.94507	16.4	0.778E-03	3.7
148	0.839	0.412E+06	0.99981	0.94369	13.3	0.741E-03	3.6
$n = 2, \Gamma = 5/3, r_p = 2.7r_t$							
317	1.63	0.640E+06	0.99987	0.95578	3.8	0.22E-03	1.9
318	1.60	0.633E+06	0.99987	0.95521	5.5	0.29E-03	2.2
319	1.69	0.656E+06	0.99987	0.95465	5.5	0.33E-03	2.3
320	1.71	0.663E+06	0.99987	0.95401	7.5	0.37E-03	2.5
321	1.88	0.706E+06	0.99988	0.95343	5.8	0.36E-03	2.4
322	1.86	0.700E+06	0.99988	0.95272	7.5	0.36E-03	2.4
...							
328	1.89	0.707E+06	0.99988	0.94854	6.3	0.40E-03	2.6
329	1.91	0.713E+06	0.99988	0.94778	4.9	0.40E-03	2.6
330	1.99	0.734E+06	0.99989	0.94703	7.4	0.43E-03	2.7
331	2.01	0.738E+06	0.99989	0.94633	8.0	0.38E-03	2.5
332	2.40	0.829E+06	0.99990	0.94533	9.2	0.57E-03	3.1
333	2.18	0.779E+06	0.99989	0.94448	8.1	0.43E-03	2.7

^aThe time unit for the orbital period is $t_u \equiv \text{yr} \lambda^{3/2} M_4^{-1/2}$, where $\lambda \equiv R/(0.01R_\odot)$ and $M_4 \equiv M_{\text{BH}}/(10^4 M_\odot)$. The unit of fallback dM/dt is $M/t_u = M_\odot \text{yr}^{-1} \mu \lambda^{-2} M_4^{1/2}$, where $\mu = M/M_\odot$. The Eddington time t_{Edd} has been calculated according to eq. (5) and is listed in units of day $(\epsilon/0.1)^{0.53} \mu^{0.53} \lambda^{0.71} M_4^{-0.76}$, where ϵ is the radiative efficiency.